

Qubit Metrology of Ultralow Phase Noise Using Randomized Benchmarking

P. J. J. O'Malley,¹ J. Kelly,^{1,*} R. Barends,^{1,*} B. Campbell,¹ Y. Chen,^{1,*} Z. Chen,¹ B. Chiaro,¹ A. Dunsworth,¹ A. G. Fowler,^{1,2,*} I.-C. Hoi,¹ E. Jeffrey,^{1,*} A. Megrant,^{1,3} J. Mutus,^{1,*} C. Neill,¹ C. Quintana,¹ P. Roushan,^{1,*} D. Sank,^{1,*} A. Vainsencher,¹ J. Wenner,¹ T. C. White,¹ A. N. Korotkov,⁴ A. N. Cleland,¹ and John M. Martinis^{1,*}

¹*Department of Physics, University of California, Santa Barbara, California 93106, USA*

²*Centre for Quantum Computation and Communication Technology, School of Physics, The University of Melbourne, Victoria 3010, Australia*

³*Department of Materials, University of California, Santa Barbara, California 93106, USA*

⁴*Department of Electrical and Computer Engineering, University of California, Riverside, California 92521, USA*

(Received 30 October 2014; revised manuscript received 6 March 2015; published 17 April 2015)

A precise measurement of dephasing over a range of time scales is critical for improving quantum gates beyond the error correction threshold. We present a metrological tool based on randomized benchmarking capable of greatly increasing the precision of Ramsey and spin-echo sequences by the repeated but incoherent addition of phase noise. We find our superconducting-quantum-interference-device-based qubit is not limited by $1/f$ flux noise at short time scales but instead observe a telegraph noise mechanism that is not amenable to study with standard measurement techniques.

DOI: 10.1103/PhysRevApplied.3.044009

I. INTRODUCTION

One of the main challenges in quantum information is maintaining precise control over the phase of a superposition state. Long-term phase stability is threatened by frequency drifts due to non-Markovian noise, which arises naturally in solid-state quantum systems [1,2]. Fortunately, correlated noise can be suppressed using Hahn spin echo [3]. In practice, Ramsey and spin-echo measurements of dephasing [4–6] characterize the dominant noise source for large error rates (0.1 to 0.5) and long times but are fundamentally inappropriate for understanding noise dominant on the time scales and error rates needed for fault-tolerant gate operations ($< 10^{-2}$).

In this article, we introduce a metrological tool based on randomized benchmarking (RB) [7–12] to quantify noise on time scales relevant for quantum gates. Whereas other measurement techniques based on Ramsey [4–6] and Rabi [13] measurements measure noise over long time scales and filter low-frequency noise to infer gate performance at short time scales, we measure gate fidelity directly, providing immediate feedback on the impact of noise on gate performance. We apply it on a superconducting-quantum-interference-device- (SQUID)-based qubit and show that this method determines that $1/f$ flux noise [1,14,15] is not currently a limiting factor in our device. This tool also provides a powerful probe of anomalous telegraph noise sources seen in superconducting devices. We also show that undesired coherent interactions can be understood as an effective correlated noise. Finally, we

demonstrate how this method allows for error budgeting and direct selection of ideal gate parameters in the presence of non-Markovian noise.

Quantum systems based on ion traps, spin qubits, and superconducting circuits are rapidly maturing, with individual operation fidelity at the levels required for fault-tolerant quantum computing [10,16–24]. These systems are often limited by environmentally induced phase noise, which can manifest as qubit frequency jitter. Noise in the phase ϕ is characterized by variance $\langle \phi^2(\tau) \rangle$, increasing linearly with time τ for white noise and with higher power for correlated noise [25]. Ramsey and spin-echo experiments measure the decay of phase coherence for large magnitudes over long time scales; at much shorter time scales, which are relevant to quantum gates but still slower than the qubit frequency, dephasing errors are small and, thus, hard to measure, making physical mechanisms difficult to directly identify. Here, we quantify phase noise by using RB to measure the decoherence of an identity gate vs its duration, providing an unprecedented metrological tool.

We use a superconducting quantum system based on the planar transmon qubit variant, the Xmon [26], cooled to 20 mK in a dilution refrigerator. This qubit consists of a SQUID, which serves as a tunable nonlinear inductor and a large X-shaped shunt capacitor. It is well suited for characterizing phase noise as the qubit has long energy-relaxation times, and the SQUID gives a controllable susceptibility to flux noise. These qubits have frequencies that can be tuned to 6 GHz and below and have typical nonlinearities of $\eta/2\pi = -0.22$ GHz, and capacitive coupling strengths between qubits of $2g/2\pi = 30$ MHz [27].

*Present address: Google Inc., Santa Barbara, California 93117, USA.

Single-qubit rotations are performed with microwave pulses and tuned using closed-loop optimization with RB [28]. We use a dispersive readout scheme with capacitively coupled resonators at 6.6–6.8 GHz for state measurements [29]. For details of the experiment setup and fabrication process, see Ref. [24].

II. RB RAMSEY EXPERIMENT

Figure 1(a) shows gate sequences for Ramsey and spin-echo measurements, as well as their RB equivalents that we call “RB Ramsey” and “RB echo.” The Ramsey experiment accumulates phase error from a single period τ , whereas the RB Ramsey experiment accumulates phase error from m applications of τ , with m typically of order 100. In RB, gate error is measured directly by interleaving gates with random Clifford group operators, which depolarize errors by evenly sampling the Hilbert space, such that repeated gate applications add error incoherently [30]. Thus, the RB Ramsey experiment has a factor m higher sensitivity than the Ramsey experiment when errors and times τ are small. The error of an idle gate $r_{I(\tau)}$ is directly related to the variance of the phase noise by (see Appendix A)

$$r_{I(\tau)} = \frac{1}{6} \langle \phi^2(\tau) \rangle. \quad (1)$$

We infer and plot the equivalent Ramsey decay envelope visibility data V (solid circles) with $V(\tau) = A \exp[-\frac{1}{2} \langle \phi^2(\tau) \rangle] + B$ in Fig. 1(b), with state preparation and measurement error parameters A and B extracted from the Ramsey fit as described in Appendix C and $\langle \phi^2(\tau) \rangle$ measured by the RB Ramsey experiment according to Eq. (1). We likewise show the equivalent spin-echo decay envelope from RB echo data as solid squares. The Ramsey and spin-echo measurements over the same time scale are shown for comparison as open circles and open squares, respectively. We label the length of a single-qubit and two-qubit entangling gate [23] to emphasize the relevant time scale. The full Ramsey and spin-echo measurements are shown on the typical linear scale together with energy relaxation in the inset of Fig. 1(b).

As shown in Fig. 1(b), the RB Ramsey and RB echo data are consistent with the Ramsey and spin-echo measurements, respectively, at short to moderate time scales, while being much more precise. Any structure to short-time dephasing is obscured in the Ramsey data, whereas the RB Ramsey data reveal a time dependence that we will show is consistent with telegraph noise. The use of RB greatly improves the precision of phase-noise measurements; the uncertainty of the measured Ramsey visibility for $\tau < 300$ ns is reduced by an order of magnitude. We note that the total time taken to perform the Ramsey and RB Ramsey measurements is approximately the same and that precision will be increased for a higher-fidelity qubit by simply choosing larger m 's. Because of the imprecision of the Ramsey data at short time scales, the amount of noise

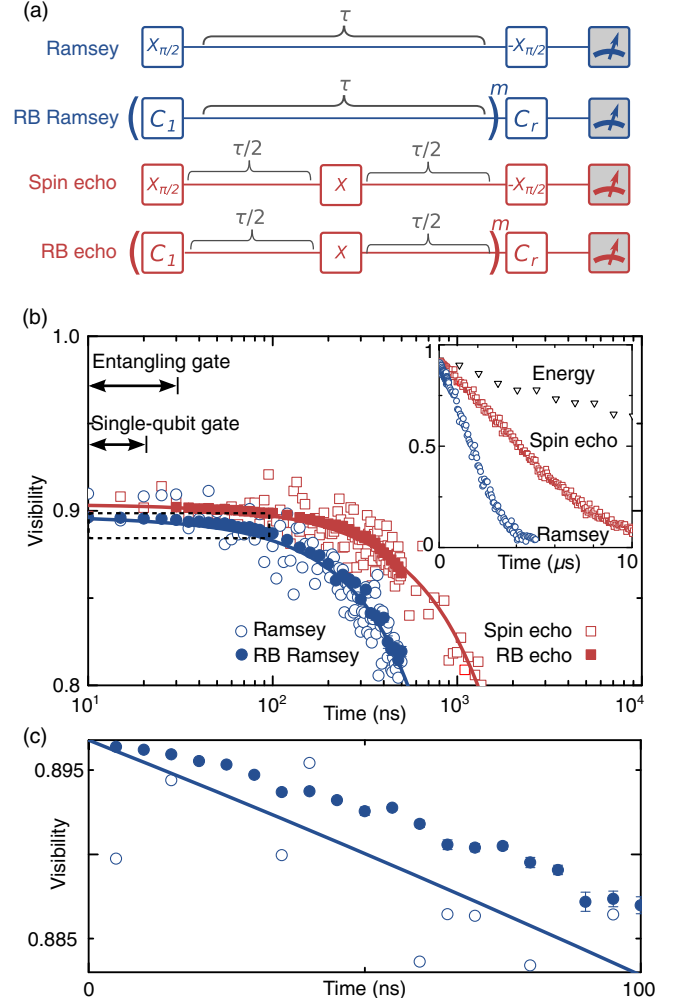


FIG. 1. (a) Gate diagram for Ramsey and Hahn spin-echo sequences and their RB equivalents. For the RB Ramsey sequence, instead of inserting an idle gate between $X_{\pi/2}$ pulses, we interleave the idle gate between m randomly selected single-qubit Clifford gates (C_1), after which the qubit is rotated back (C_r) to the pole and measured. For spin echo and RB echo, an X gate is inserted at the center of the idle sequence. The range of m is 21 for the longest τ to 300 for the shortest. (b) (inset) T_1 (energy decay) and Ramsey and spin-echo envelopes; (main) Ramsey (open circle) and spin-echo (open square) envelopes at short times. RB decay envelopes are inferred from $\langle \phi^2(\tau) \rangle$ measured by the RB Ramsey (solid circle) and RB echo (solid square) experiments; see text for details. Single-qubit and entangling gate durations are shown for reference. Note the significantly lower noise of the RB sequences, which take approximately the same measurement time as the Ramsey and echo experiments. (c) Magnification of the dashed area in (b), showing time scales important for gates. The RB Ramsey data show a trend different from that predicted by the Ramsey fit.

present can be inferred only from the fit to the entire Ramsey data set. However, Fig. 1(c) shows that the phase noise measured by the RB Ramsey experiment can differ significantly from that expected by the Ramsey fit. The trend in their difference indicates that there is behavior to

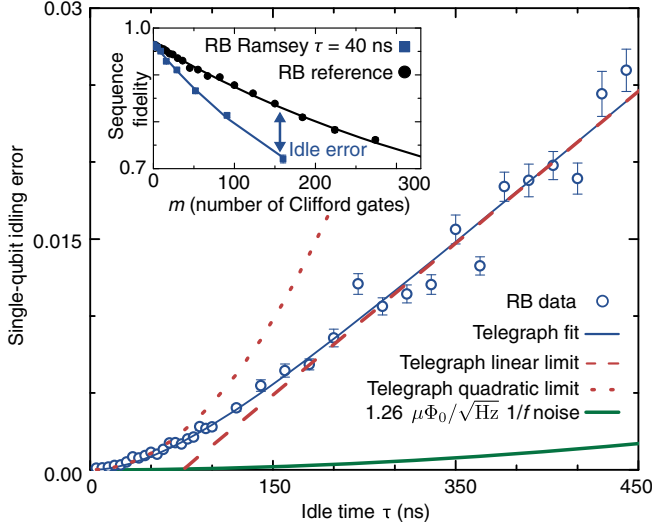


FIG. 2. RB Ramsey measurement (circles) for short time scales; note that the small error from T_1 decay, which is 9×10^{-4} at 450 ns, is subtracted (see Appendix A). We fit to a telegraph noise model [Eq. (4)]; the dotted (dashed) lines give the short (long) time limit of the noise model. The inferred but negligible contribution from $1/f$ noise as measured for this qubit (see Appendix D) is shown as a thick line. The inset shows the sequence fidelity vs the number of Clifford gates, with and without interleaved idle gates used to extract the idle gate error for $\tau = 40$ ns.

the noise at short times that Ramsey measurements miss. We examine this in Fig. 2.

III. MEASURING TELEGRAPH NOISE

To identify the dominant noise mechanism, we examine the dependence of idle gate error on time and compare against different noise models in Fig. 2. Whereas in Fig. 1 we infer an equivalent Ramsey envelope, here we plot the idle gate error directly, as measured by the RB Ramsey experiment (with small T_1 effects subtracted; see Appendix A). For short times, we see a nonlinear increase of error with gate duration which transitions into a linear behavior for lengths above approximately 100 ns. The inset shows the sequence fidelity vs the number of Clifford gates, with and without interleaved idle gates used to extract the idle gate error for $\tau = 40$ ns.

While it has long been known that SQUIDs are susceptible to $1/f$ flux noise [1,14,31–35], we find this is a negligible contribution to gate error. A system limited by $1/f$ and white noise will see a linear increase in error at short times and quadratic increase at long times as the $1/f$ component begins to dominate. The data exhibit the opposite trend. Moreover, the expected contribution to gate error from $1/f$ noise, as measured for this system below 1 Hz using the Ramsey tomography oscilloscope protocol (see Ref. [14] and Appendix D), is significantly less than observed here (Fig. 2 thick solid line).

The trend observed in Fig. 2 is consistent with telegraph noise. For a random telegraph switching of the qubit frequency, the phase noise is given by

$$\langle \phi_{\text{tel}}^2(\tau) \rangle = (2\pi\Delta f_{10})^2 T_{\text{sw}} \left\{ \tau - T_{\text{sw}} \left[1 - \exp\left(-\frac{\tau}{T_{\text{sw}}}\right) \right] \right\}, \quad (2)$$

where Δf_{10} is the effective switching amplitude of the qubit frequency, and T_{sw} is the switching time scale. We make the simplifying assumption of symmetric telegraph noise as the measurement is unable to differentiate up and down switching rates, and note that while telegraph noise is not Gaussian, Eq. (2) is still approximately correct for use in Ramsey and spin-echo analyses (see Appendix A). In a more general case, the error rate for an idle gate of length τ , $r_{I(\tau)}$, can be fit to a combination of error sources: white, long-time correlated, $1/f$, and telegraph phase noise, as well as T_1 decay,

$$r_{I(\tau)} = \frac{\tau}{3T_1} + \frac{1}{6} \{ \langle \phi_{\text{white}}^2(\tau) \rangle + \langle \phi_{\text{corr}}^2(\tau) \rangle + \langle \phi_{1/f}^2(\tau) \rangle + \langle \phi_{\text{tel}}^2(\tau) \rangle \}, \quad (3)$$

where the derivation for $\langle \phi_{\text{white}}^2(\tau) \rangle = 2\tau/T_{\phi_1}$, $\langle \phi_{\text{corr}}^2(\tau) \rangle = 2(\tau/T_{\phi_2})^2$, and $\langle \phi_{1/f}^2(\tau) \rangle$ are given in Appendix B, and we assume correlated noise has a longer time scale than the experiment. The data here are fitted to a noise model featuring only T_1 decay (measured independently) and telegraph noise,

$$r_{I(\tau)} = \frac{\tau}{3T_1} + \frac{1}{6} \langle \phi_{\text{tel}}^2(\tau) \rangle, \quad (4)$$

indicating that $1/f$ and white noise do not dominate the error for this qubit. We extract $T_{\text{sw}} = 84 \pm 14$ ns and $\Delta f_{10} = 479 \pm 30$ kHz from the fit. The dotted (dashed) line shows this noise model in the short (long) time limit. Perhaps surprisingly, this measurement directly shows that gates of duration 20 ns can achieve fidelity > 0.999 in a system with characteristic Ramsey scale of $T_{\phi_2} = 2.0 \mu\text{s}$ (see Appendix C).

Telegraph noise has been studied in superconducting circuits with a variety of methods. Frequency fluctuations due to quasiparticle tunneling have been characterized by Rabi oscillations [36] and repeated direct frequency measurement [37]. For our qubit, the calculated frequency splitting due to quasiparticle tunneling ranges from 1 Hz to 14 kHz (see Appendix F), well below the magnitude necessary to explain the data. Photon shot noise in a coupled resonator has been shown to cause dephasing in both transmon [17,18,38] and flux [39] qubits. In our case, the magnitude of the telegraph noise decreases as the qubit-resonator frequency difference decreases, indicating that resonator photon noise-induced dephasing is not the cause. A more elusive telegraphlike noise has been measured by $T_{1\rho}$ Rabi spectroscopy in flux qubits [13], hypothesized to be due to two sets of coupled coherent two-level states. This noise is similar in frequency to the noise measured

here, with spectroscopic signatures at 1 and 20 MHz, compared to $1/84 \text{ ns} = 11 \text{ MHz}$ for this measurement. However, it is much larger in magnitude, presenting as a “dip” (or “plateau”) in spin-echo measurements, which is known to happen in the presence of strong telegraph noise [40] and seen in other systems [37,39,41]. In our device, the telegraph noise is only dominant at short time scales, as any evidence of it in longer measurements like the Ramsey measurement and spin echo is masked by $1/f$ flux noise.

IV. MEASURING ERROR FROM COHERENT QUBIT-QUBIT INTERACTIONS

We now apply RB to coherent errors arising from unwanted qubit-qubit interactions, which can also contribute to dephasing [42]. In Fig. 3, we explore these effects in our system. Figure 3(a) shows an energy-level diagram for capacitively coupled qubits, where the fundamental entangling rate Ω_{ZZ} [43] arises from an avoided level crossing between the $|11\rangle$ state and the $|02\rangle$ and $|20\rangle$ states. This interaction manifests as a state-dependent frequency shift falling off with detuning Δ , as measured in Fig. 3(b). We note that for a qubit coupled to a resonator Ω_{ZZ} is equivalent to the dispersive shift [44] 2χ as defined in Ref. [45]. The inability to turn this interaction off completely results in additional errors when operating qubits

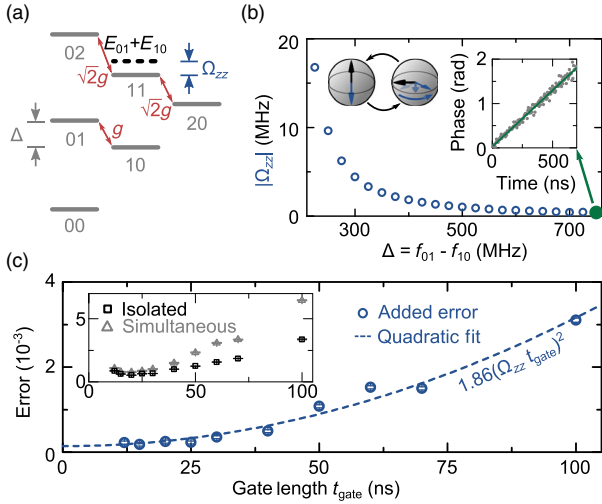


FIG. 3. (a) Energy-level diagram for two capacitively coupled qubits with coupling strength $2g/2\pi = 30 \text{ MHz}$, detuned by frequency Δ . The avoided level crossing between the $|11\rangle$ and the $|02\rangle$ and $|20\rangle$ states repels the $|11\rangle$ frequency from the sum of $|01\rangle$ and $|10\rangle$ frequencies by the amount Ω_{ZZ} . (b) This entangling interaction causes the phase of one qubit to precess, conditional on the state of its neighbor (sketch and inset). The Ω_{ZZ} interaction decreases with Δ , to a level of $\Omega_{ZZ}/2\pi = 0.4 \text{ MHz}$ at $\Delta/2\pi = 750 \text{ MHz}$. (c) RB data isolating the Ω_{ZZ} interaction. Gate error is measured vs gate duration for a single qubit and when qubits are operated simultaneously (inset). The difference (main figure) measures the error contribution from the Ω_{ZZ} interaction and is fit to $1.86(\Omega_{ZZ}t_{\text{gate}}/2\pi)^2 + 1.4 \times 10^{-4}$.

simultaneously. Figure 3(c) shows the average gate error vs duration when a qubit is operated in isolation or simultaneously with a coupled qubit ($\Omega_{ZZ}/2\pi = 0.4 \text{ MHz}$). The error for a single qubit or simultaneous operation is inferred from the RB reference error per Clifford gate divided by the average of 1.875 physical gates per Clifford gate [23]. The difference between isolated and simultaneous operation gives the added error from the Ω_{ZZ} interaction, which is fit to a quadratic.

This interaction is correlated, and, therefore, the errors are quadratic with gate duration; specifically, the error per gate due to the Ω_{ZZ} interaction between two qubits simultaneously undergoing RB is

$$E = \frac{\pi^2}{6} \left(\frac{\Omega_{ZZ}}{2\pi} t_{\text{gate}} \right)^2, \quad (5)$$

where $\Omega_{ZZ}/2\pi$ is the interaction magnitude, and t_{gate} is the RB gate duration (see Appendix G). The fit to the data has a quadratic coefficient of 1.86 ± 0.1 , while $\pi^2/6 \approx 1.64$. Here, the careful application of RB both distinguishes these errors at the 1×10^{-4} level and indicates that short gates are effective in suppressing them.

V. MEASURING DIFFERENT GATE IMPLEMENTATIONS

We now examine the gate fidelity for a variety of gates in the presence of the non-Markovian noise we have measured. Figure 4 shows gate fidelity vs gate length for two implementations each of two different gates: for σ_I , an idle and two microwave pulses (X, X), and for σ_Z , a frequency detuning pulse and two microwave pulses (Y, X). The errors of these operations vs duration are determined with interleaved RB. In agreement with previous measurements,

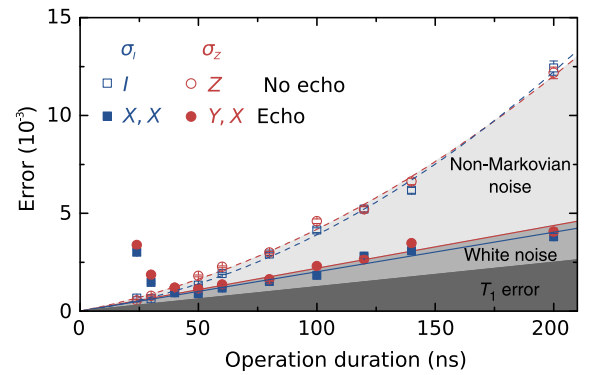


FIG. 4. Operation error of σ_I and σ_Z , implemented with (closed symbols) and without (open symbols) echoing, as measured with interleaved RB. The data are fitted to a linear and quadratic form representing uncorrelated and correlated noise. The dark gray region indicates error attributed to T_1 , the medium gray region uncorrelated noise, and the light gray region non-Markovian (e.g., telegraph) noise. Note that the I data are RB Ramsey data, the same as Fig. 2.

we find that the error of operations without X or Y pulses (open symbols) follows a quadratic dependence with gate duration at these time scales. Using X or Y pulses (closed symbols), we observe a linear dependence at longer durations, indicating that the correlated phase noise is suppressed. Below 40 ns, we find an increased error, which we attribute to the population of higher levels due to spectral leakage [46]. The solid (dashed) lines are linear (linear and quadratic) fits to the data. For full details of the fits, see Appendix C.

Using the functional forms of the different error types given in Eq. (3), we can determine an error budget for our operations. For a typical entangling gate duration of 40 ns, T_1 contributes an error of 5×10^{-4} and telegraph noise an error of 5×10^{-4} . With echoing pulses, the total error is 8×10^{-4} , indicating that the added echoing pulses are either not completely suppressing the phase noise or are contributing error of their own. Using a combination of RB Ramsey and RB echo measurements, we determine the relative contribution of different noise sources to operational error, and we can also immediately see that either short gates or long gates with intrinsic echoing are effective at remedying non-Markovian noise, and by how much.

VI. SUMMARY

The RB Ramsey experiment provides a direct measurement of phase noise in the regime most relevant to quantum gates. While previous noise spectroscopy has relied on accumulating noise over longer time scales while filtering out low-frequency noise with additional pulses, our technique directly measures small amounts of noise with repeated incoherent additions. It does not require extensive calibration and is also robust against state preparation and measurement error. As a gate-based measurement, it is useful in a variety of situations: measuring noise due to the environment of the RB Ramsey experiment, measuring filtered environmental noise as RB echo, and measuring dephasing induced by coherent qubit-qubit interactions. As the measurement output is gate fidelity, it is also immediately applicable as a tool to determine the highest-fidelity implementation of different quantum gates in the presence of noise. We show here that the RB Ramsey experiment is the metrological tool best suited for measuring noise in high-fidelity qubits.

We take RB, a protocol for determining the fidelity of gates, and apply it as a metrological tool for identifying noise processes. Applied to a superconducting qubit system, we find a telegraph noise mechanism in a regime inaccessible to previous measurements, accurately characterize dephasing caused by coherent qubit-qubit interactions, and determine the highest-fidelity implementation of different quantum gates. Our results demonstrate that the RB Ramsey experiment is capable of measuring small noise processes at short time scales that are directly relevant to gate fidelity and show that understanding this

non-Markovian phase noise can lead to its effective suppression through short gates and echoing.

ACKNOWLEDGMENTS

We thank A. Veitia for helpful discussions on the theory of noise and RB. This work is supported by the Office of the Director of National Intelligence (ODNI), Intelligence Advanced Research Projects Activity (IARPA) through the Army Research Office Grants No. W911NF-09-1-0375 and No. W911NF-10-1-0334. All statements of fact, opinion, or conclusions contained herein are those of the authors and should not be construed as representing the official views or policies of IARPA, the ODNI, or the U.S. government. Devices are made at the UC Santa Barbara Nanofabrication Facility, a part of the NSF-funded National Nanotechnology Infrastructure Network, and at the NanoStructures Cleanroom Facility.

P.J.J.O., J.K., and R.B. contributed equally to this work.

APPENDIX A: THEORETICAL RELATION OF RB ERROR TO $\langle \phi^2 \rangle$

In order to determine the effect of various dephasing mechanisms on a RB sequence, we first consider the following simplified model: a single qubit begins in $|\psi_0\rangle = |0\rangle$, then a randomly chosen perfect Clifford rotation C_1 is applied, and then a phase $\phi_{g,n}$ is accumulated by application of a Z rotation to simulate phase noise. The random Clifford and noise gate pair are repeated N times, after which the single Clifford gate C_r , that is the inverse of all the previous Clifford gates is applied to rotate back to (nearly) $|0\rangle$, and we measure the probability of error, $P_{\text{err}} = |\langle 1 | \psi_N \rangle|^2$.

The value of $\phi_{g,n}$ depends on the dephasing model employed. For example, for static dephasing (e.g., a frequency offset), it is constant: $\phi_{g,n} = \phi_{g,\text{st}}$. For white noise, $\phi_{g,n}$ is randomly sampled from a symmetric Gaussian distribution. In general, $\phi_{g,n}$ is arbitrary, but we assume $|\phi_{g,n}| \ll 1$. The average square of $\phi_{g,n}$ is denoted $\langle \phi_g^2 \rangle$.

We now consider the “error angle” $\Delta\phi$ the angular separation of $|\psi_N\rangle$ from $|0\rangle$ in the Bloch sphere picture of a single qubit, noting that $P_{\text{err}} = \langle (\Delta\phi/2)^2 \rangle$, assuming $|\Delta\phi| \ll 1$. Because $|\phi_{g,n}| \ll 1$ and N is not too large, after each rotation, $|\psi\rangle$ is close to one of the six axes ($\pm X, \pm Y, \pm Z$), and the angular distance from the axis is $\Delta\phi$. There is a 1/3 chance that the qubit is near the pole (i.e., Z axis) and then the rotation $\phi_{g,n}$ does not change $\Delta\phi$, while with a 2/3 probability the qubit is near the equator and $\Delta\phi$ is changed.

For any dephasing model, it is straightforward to see that the evolution of $\Delta\phi$ is essentially a random walk in two dimensions and that

$$\langle(\Delta\phi)^2\rangle = \frac{2}{3}N\langle\phi_g^2\rangle, \quad (\text{A1})$$

assuming $N\langle\phi_g^2\rangle \ll 1$. The RB error is then

$$P_{\text{err}} = \langle(\Delta\phi/2)^2\rangle = \frac{1}{6}N\langle\phi_g^2\rangle. \quad (\text{A2})$$

It might be expected that in the static dephasing case—when there are correlated phase contributions—there can be some sort of echoing effect; for example, if a Clifford gate takes $|\psi\rangle$ to the $+Y$ axis and it is rotated by $\phi_{g,\text{st}}$, then if the next Clifford gate is an X rotation putting $|\psi\rangle$ near the $-Y$ axis, the following rotation also by $\phi_{g,\text{st}}$ will cancel the previous noise rotation. However, when the full set of Clifford rotations is used, there are four rotations that take $|\psi\rangle$ near the $-Y$ axis, and each orients the previous $\Delta\phi$ in a different direction relative to the axis, resulting in equal probability of canceling the previous rotation, doubling it, or moving in one of the two perpendicular directions. The noise accumulated between rotations is, therefore, uncorrelated with previous or future noise; the Clifford set is error depolarizing. Therefore, Eqs. (A1) and (A2) hold regardless of the noise model.

This simplified model is confirmed with simulation for both a static and an uncorrelated noise model with $\phi_{g,n} = \pm\phi_g$.

This implies that RB is an effective way to measure dephasing if the sequence error occurring between the gates is attributable to dephasing. This can be done easily by comparing the sequence fidelity of a RB sequence with an interleaved idling time to that of a reference RB sequence, effectively subtracting out errors due to the Clifford gates themselves—in other words, measuring the fidelity of an idle gate using interleaved RB, as in Ref. [23]. We can, therefore, measure the dephasing that takes place during an idle gate period and by varying the length τ of an idle gate period measure dephasing as a function of time, $\langle\phi^2(\tau)\rangle$ (for brevity, we remove the subscript g). With $r_{I(\tau)}$ being the error rate (i.e., error per gate) of an idle gate period we, thus, arrive at Eq. (1),

$$P_{\text{err}}/N = r_{I(\tau)} = \frac{1}{6}\langle\phi^2(\tau)\rangle. \quad (\text{A3})$$

For completeness, we also mention here the effect of energy relaxation (T_1 decay) on the fidelity of RB sequences. After each Clifford gate, the qubit state $|\psi\rangle$ is near the equator of the Bloch sphere with probability $2/3$. In this case, the probability of the energy-relaxation event is $\tau/2T_1$ (we assume $\tau \ll T_1$); such an event moves $|\psi\rangle$ by approximately the angle $\pi/2$ on the Bloch sphere, thus, leading to the error probability $1/2$ at the end of the RB sequence. The corresponding contribution to the RB error per gate is $(2/3) \times (\tau/2T_1) \times (1/2) = \tau/6T_1$. With probability $1/6$, the qubit state after a Clifford gate is close to the north pole (state $|0\rangle$); then there is no energy relaxation. Finally, with probability $1/6$, the qubit state is close to the south pole $|1\rangle$;

then the probability of the energy-relaxation event is τ/T_1 , which moves the state by approximately the angle π , thus, almost certainly leading to the RB error. The corresponding contribution to the RB error per gate is $(1/6) \times (\tau/T_1) \times 1 = \tau/6T_1$. Adding together the two contributions, we arrive at

$$P_{\text{err}}/N = \frac{\tau}{3T_1}. \quad (\text{A4})$$

Since T_1 can be measured independently, the effects of T_1 decay can be calculated and subtracted from the results obtained with RB, much as it can be subtracted from Ramsey visibility decays as well. In our experiment, T_1 is relatively large, and, therefore, this correction is small.

APPENDIX B: TYPES OF PHASE NOISE

We now discuss the form of $\langle\phi^2(\tau)\rangle$ for different sources of noise. For completeness, we also show the similar characteristic, $\langle\tilde{\phi}^2(\tau)\rangle$, for the echo sequence of duration τ (with π pulse at $\tau/2$). Most of the results discussed here were presented earlier, e.g., in Refs. [4, 25, 33].

The average values $\langle\phi^2(\tau)\rangle$ and $\langle\tilde{\phi}^2(\tau)\rangle$ for the idle and echo sequence, respectively, can be calculated via the spectral density $S(\omega)$ of the qubit frequency fluctuation,

$$\langle\phi^2(\tau)\rangle = \tau^2 \int_0^\infty S(\omega) \left[\frac{\sin(\omega\tau/2)}{\omega\tau/2} \right]^2 \frac{d\omega}{2\pi}, \quad (\text{B1})$$

$$\langle\tilde{\phi}^2(\tau)\rangle = \tau^2 \int_0^\infty S(\omega) \frac{\sin^4(\omega\tau/4)}{(\omega\tau/4)^2} \frac{d\omega}{2\pi}, \quad (\text{B2})$$

where $S(\omega)$ is single sided, and the average frequency fluctuation is assumed to be zero.

For the white noise with a flat spectral density $S(\omega) = S_0$, we find

$$\langle\phi_{\text{white}}^2(\tau)\rangle = \langle\tilde{\phi}_{\text{white}}^2(\tau)\rangle = \frac{S_0}{2}\tau = 2\frac{\tau}{T_{\phi_1}}, \quad (\text{B3})$$

where $T_{\phi_1} = 4/S_0$ is the dephasing time due to white noise. Note that the factor of 2 in the last expression cancels when the corresponding visibility of a Ramsey or echo sequence $\exp(-\tau/T_{\phi_1})$ is calculated.

For noise that is correlated over very long times (very slowly fluctuating qubit frequency), $S(\omega) = 4\pi\sigma_{\text{qb}}^2\delta(\omega)$, where σ_{qb} is the standard deviation of the qubit frequency $2\pi f_{10}$. In this case,

$$\langle\phi_{\text{corr}}^2(\tau)\rangle = \sigma_{\text{qb}}^2\tau^2 = 2\left(\frac{\tau}{T_{\phi_2}}\right)^2, \quad \langle\tilde{\phi}_{\text{corr}}^2(\tau)\rangle = 0, \quad (\text{B4})$$

where $T_{\phi_2} = \sqrt{2}/\sigma_{\text{qb}}$ is the Ramsey dephasing time scale due to such correlated noise. Obviously, in this case there is no dephasing in the echo sequence visibility.

For $1/f$ noise, let us use $S(\omega) = (S_{1/f})/(\omega/2\pi)$, then [25,33]

$$\langle \phi_{1/f}^2(\tau) \rangle = S_{1/f} \tau^2 \ln \frac{0.4007}{f_c \tau}, \quad (\text{B5})$$

$$\langle \tilde{\phi}_{1/f}^2(\tau) \rangle = S_{1/f} \tau^2 \ln 2, \quad (\text{B6})$$

where $f_c = \omega_c/2\pi$ is the low-frequency cutoff of the $1/f$ noise (e.g., the inverse of the total duration of the experiment), which is introduced as the lower limit of integration in Eq. (B1). Note that in Eq. (B5), we assumed $f_c \tau \lesssim 0.2$. As the log part in Eq. (B5) varies slowly, typically it is ignored, and $1/f$ noise for $\langle \phi^2(\tau) \rangle$ is treated with Eq. (B4). Note that the factors in Eqs. (B5) and (B6) are different, resulting in different effective dephasing times T_{ϕ_2} for the Ramsey and echo sequences.

Finally, let us consider a telegraph noise, for which the qubit frequency $2\pi f_{10}$ switches between two values separated by $\Delta\omega_{\text{qb}}$, with an up (down) switching rate of Γ_{\uparrow} (Γ_{\downarrow}). In this case.

$$S(\omega) = \frac{4(\Delta\omega_{\text{qb}})^2 \Gamma_{\uparrow} \Gamma_{\downarrow}}{\Gamma_{\Sigma}(\omega^2 + \Gamma_{\Sigma}^2)}, \quad \Gamma_{\Sigma} = \Gamma_{\uparrow} + \Gamma_{\downarrow}, \quad (\text{B7})$$

so using Eqs. (B1) and (B2), we obtain

$$\langle \phi_{\text{tel}}^2(\tau) \rangle = 2 \frac{(\Delta\omega_{\text{qb}})^2 \Gamma_{\uparrow} \Gamma_{\downarrow}}{\Gamma_{\Sigma}} \left(\tau - \frac{1 - e^{-\Gamma_{\Sigma} \tau}}{\Gamma_{\Sigma}} \right), \quad (\text{B8})$$

$$\langle \tilde{\phi}_{\text{tel}}^2(\tau) \rangle = 2 \frac{(\Delta\omega_{\text{qb}})^2 \Gamma_{\uparrow} \Gamma_{\downarrow}}{\Gamma_{\Sigma}} \left(\tau - \frac{3 + e^{-\Gamma_{\Sigma} \tau} - 4e^{-\Gamma_{\Sigma} \tau/2}}{\Gamma_{\Sigma}} \right). \quad (\text{B9})$$

Note that at short time, $\tau \ll \Gamma_{\Sigma}^{-1}$, the effect of the telegraph noise is similar to the effect of the correlated noise with $T_{\phi_2} = \sqrt{2} \Gamma_{\Sigma} / (\sqrt{\Gamma_{\uparrow} \Gamma_{\downarrow}} \Delta\omega_{\text{qb}})$, while at long time, $\tau \gg \Gamma_{\Sigma}^{-1}$, it is similar to the effect of white noise with $T_{\phi_1} = \Gamma_{\Sigma}^3 / [\Gamma_{\uparrow} \Gamma_{\downarrow} (\Delta\omega_{\text{qb}})^2]$.

Defining the effective switching amplitude as $2\pi \Delta f_{10} = 2\Delta\omega_{\text{qb}} \sqrt{\Gamma_{\uparrow} \Gamma_{\downarrow}} / \Gamma_{\Sigma}$ and introducing notation $T_{\text{sw}} = 1/\Gamma_{\Sigma}$, we can rewrite Eq. (B8) as

$$\langle \phi_{\text{tel}}^2(\tau) \rangle = (2\pi \Delta f_{10})^2 T_{\text{sw}} [\tau - T_{\text{sw}} (1 - e^{-\tau/T_{\text{sw}}})], \quad (\text{B10})$$

which is Eq. (2). In the case where $\Gamma_{\uparrow} = \Gamma_{\downarrow}$, as we assume, $2\pi \Delta f_{10}$ provides a lower bound on $\Delta\omega_{\text{qb}}$. Note that the telegraph noise is not Gaussian. Therefore, while the obtained equations can be used to find the RB error per gate, they cannot, strictly speaking, be used to find the visibility of the standard Ramsey and echo sequences. Nevertheless, they can be used approximately if $|\Delta\omega_{\text{qb}}| / \min(\Gamma_{\uparrow}, \Gamma_{\downarrow}) \ll 1$, because at short time the

TABLE I. T_1 , Ramsey, and spin-echo fit parameters.

Sequence	T_{ϕ_1} (μs)	T_{ϕ_2} (μs)	A	B
Ramsey	6.8	2.8	0.88	0.015
Spin echo	15.1	7.5	0.88	0.021

accumulated phase shift is small, and the assumption of Gaussianity is not needed, while at longer time, when the phase becomes comparable to 1, the probability distribution for the phase becomes Gaussian due to a large number of switching events.

APPENDIX C: T_1 , RAMSEY, AND SPIN-ECHO FITS

The T_1 data are fit to a simple exponential, $P_1(t) = A \exp(-t/T_1) + B$, and we find $T_1 = 26.7 \mu\text{s}$. The Ramsey and spin-echo envelopes are each fit to a noise model that includes white and correlated components,

$$V(t) = A \exp[-t/T_{\phi_1} - (t/T_{\phi_2})^2] + B, \quad (\text{C1})$$

where $V(t)$ is the Ramsey or echo visibility, t is the length of the idle gate as shown in Fig. 1, T_{ϕ_1} is the white-noise dephasing time scale, T_{ϕ_2} is the correlated-noise dephasing time scale, and A and B are the result of state preparation and measurement errors. The fit parameters are given in Table I. Note that each of the fits includes the full range of data, from $0 < t < 5.0 \mu\text{s}$ for the Ramsey fit and $0 < t < 12.0 \mu\text{s}$ for echo sequences.

APPENDIX D: FLUX NOISE

Flux noise on this device, plotted in Fig. 5, is measured over the frequency range $10^{-4} < f < 1$ Hz, using the Ramsey tomography oscilloscope (RTO) protocol of repeated frequency measurements as described in Ref. [14]. Four measurements are made on this device (open markers) at three different operating points, and then

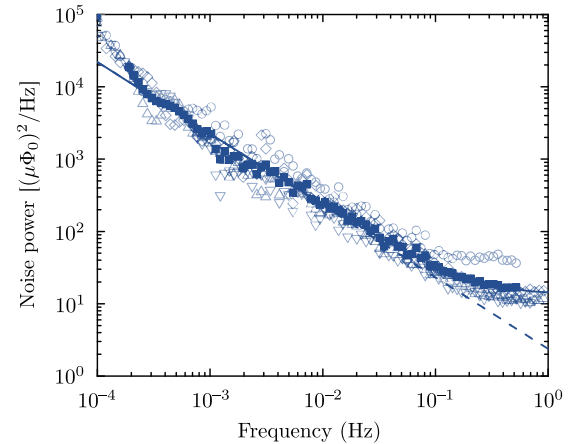


FIG. 5. Flux noise as measured with RTO [14].

each measurement is binned in logspace, and the binned measurements are averaged together (closed squares). This average is fit (solid line) to an aliased $1/f$ and white-noise model given by

$$S_\phi(f) = S_\phi^*/f^\alpha + S_\phi^*/(2f_n - f)^\alpha + S_{\text{white}}, \quad (\text{D1})$$

where $S_\phi(f)$ is the flux-noise power expressed in $(\mu\Phi_0)^2/\text{Hz}$, f is the noise frequency, α is the slope of the noise (1 for pure $1/f$ noise), S_ϕ^* is the flux-noise power at 1 Hz, $f_n = 1$ Hz is the Nyquist frequency of the measurement, and S_{white} is the white-noise floor. From the fit, we extract $S_\phi^* = 2.4(\mu\Phi_0)^2$, $\alpha = 0.99$, and $S_{\text{white}} = 9.7(\mu\Phi_0)^2/\text{Hz}$. We attribute the white noise to state preparation and measurement error. The dashed line shows the $1/f$ fit extended to 1 Hz, where the value of the y intercept is S_ϕ^* .

To plot the inferred flux-noise contribution in Figs. 2 and 6, we use Eq. (B5), with $S_{1/f} = (\partial f/\partial\phi)S_\phi^*$ taken from the measurements above, and $f_c = 10$ min the length of the experiment. The value of the log factor of Eq. (B5) varies from 13 to 7 for $1 < \tau < 450$ ns.

This analysis assumes that the low-frequency flux noise measured here can be extrapolated to high frequencies. In Fig. 2, however, we see that this calculation underestimates the amount of high-frequency noise, and furthermore, that the noise is telegraph in nature, not $1/f$.

APPENDIX E: RB RAMSEY MEASUREMENTS ACROSS THE QUBIT SPECTRUM

Figure 6 shows the RB Ramsey measurements at three additional qubit frequencies; the data for the 4.9-GHz operating point are the same as in Fig. 2. The inset shows the frequency-flux relation for this qubit, with the four operating points denoted by symbols; $df/d\phi$ changes by a factor of 2.7 between the operating points to explore different susceptibilities to flux noise. The remaining three data sets are fit to a noise model incorporating telegraph and white noise; that is,

$$r_I(\tau) = 1/6[\langle\phi_{\text{tel}}^2(\tau)\rangle + \langle\phi_{\text{white}}^2(\tau)\rangle] \quad (\text{E1})$$

[see Eqs. (B3) and (B9)]. We show the fit parameters in Table II.

TABLE II. Telegraph fit parameters.

f_{10} (GHz)	$df/d\Phi$ (GHz/ Φ_0)	T_1 (μs)	T_{ϕ_1} (μs)	T_{sw} (ns)	Δf_{10} (kHz)
5.1	3.39	30.6	20.6	182 000	184
4.9	4.81	26.7	...	84	479
4.5	6.95	31.3	12.4	98	484
4.0	9.23	36.2	15.5	263	469

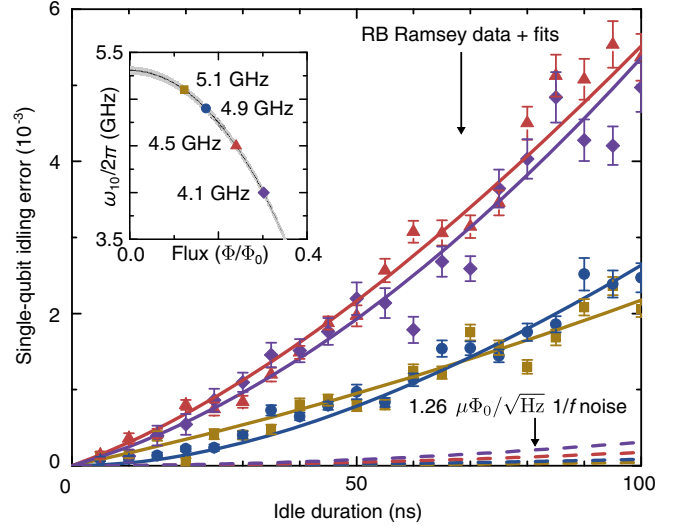


FIG. 6. RB Ramsey idling error vs duration for various frequencies; T_1 effects are subtracted according to Eq. (A4). The dashed lines denote the inferred contribution from $1/f$ flux noise at the four different operating points. The inset shows frequency spectroscopy vs applied flux, following the expected dependence [45]; the four operating points are shown.

We note that at the highest qubit frequency, the large T_{sw} indicates that the telegraph noise model is not needed here and can be replaced by the correlated-noise model with $T_{\phi_2} = \sqrt{2}/(2\pi\Delta f_{10}) = 1.2 \mu\text{s}$. The Ramsey data for this frequency, fit to Eq. (C1), give $T_{\phi_1} = 10.7 \mu\text{s}$ and $T_{\phi_2} = 3.6 \mu\text{s}$, which indicates that even though the telegraph dephasing source is not present at this operating point, the dephasing magnitude measured by the Ramsey experiment still does not match that found with RB.

Despite tuning the flux Φ/Φ_0 over most of its range, we find that $1/f$ noise does not contribute appreciably to gate errors. For typical gates of length 20 ns, idle fidelities greater than 0.999 are seen over the frequency range, demonstrating that tunable qubits can achieve high fidelity even when biased significantly away from the flux-insensitive operating point.

APPENDIX F: CHARGE NOISE

To calculate the expected frequency fluctuation due to charge noise, we use Eq. (2.5) from Ref. [45],

$$\epsilon_m \approx (-1)^m E_C \frac{2^{4m+5}}{m!} \sqrt{\frac{2}{\pi}} \left(\frac{E_J}{2E_C}\right)^{\frac{m}{2} + \frac{3}{4}} e^{-\sqrt{8E_J/E_C}}, \quad (\text{F1})$$

where ϵ_m is the charge dispersion for energy level m , and E_J and E_C are the Josephson energy and charging energy, respectively, of the qubit. Note that we can also write $E_J/E_C \approx (\omega_{01}/\eta - 1)^2/8$ [following from Eq. (2.11)], where $\omega_{01}/2\pi$ is the qubit frequency and the qubit anharmonicity $f_{12} - f_{01} = \eta/2\pi = -215 \text{ MHz}$. We then

calculate ϵ_1 for the two ends of the qubit spectrum; we find $\epsilon_1(\omega_{01}/2\pi = 6 \text{ GHz}) = 3.6 \text{ Hz}$ and $\epsilon_1(\omega_{01}/2\pi = 4 \text{ GHz}) = 14.4 \text{ kHz}$, both of which are far below the measured charge-noise fluctuation frequency of approximately 500 kHz. We also note the qubits used in Ref. [37] have charge-noise fluctuations of the same order as the telegraph noise measured here, but charge noise of that magnitude is expected, as explained by the different parameter range of those qubits: $\omega_{01}/2\pi = 4.387 \text{ GHz}$ and $\eta/2\pi = -334 \text{ MHz}$, giving $\epsilon_1 \approx 2 \text{ MHz}$.

APPENDIX G: CALCULATION OF Ω_{ZZ}

Two capacitively coupled qubits have an XX -type coupling of the form $g(|01\rangle\langle 10| + |10\rangle\langle 01|)$, where the coupling constant g is half the swap rate between the qubits. The interaction between the higher levels, $\sqrt{2}g(|11\rangle\langle 20| + |02\rangle\langle 11|) + \sqrt{2}g(|11\rangle\langle 20| + |02\rangle\langle 11|)$, results in a repulsion of the $|11\rangle$ level from the $|02\rangle$ and $|20\rangle$ levels; this energy shift in the $|11\rangle$ level produces a ZZ -type interaction between the qubits. In the far-detuned limit, neglecting the XX -coupling, the two-qubit Hamiltonian becomes

$$H = \omega_1|10\rangle\langle 10| + \omega_2|01\rangle\langle 01| + (\omega_1 + \omega_2 + \Omega_{ZZ})|11\rangle\langle 11|, \quad (\text{G1})$$

$$\Omega_{ZZ} = \frac{2g^2}{\Delta - \eta_2} + \frac{2g^2}{-\Delta - \eta_1}, \quad (\text{G2})$$

where ω_n and η_n are the qubit frequencies and non-linearities, respectively, and $\Delta = \omega_1 - \omega_2$. In our system, $\eta_1 = \eta_2 \equiv \eta$, giving

$$\Omega_{ZZ} = \frac{4g^2\eta}{\Delta^2 - \eta^2}. \quad (\text{G3})$$

When both qubits are simultaneously performing a RB sequence, phase error ϕ per idle gate in qubit A is

$$\phi = \pm \frac{\Omega_{ZZ}}{2} t_{\text{gate}}, \quad (\text{G4})$$

where t_{gate} is the idle gate duration, and the frequency shift $\pm\Omega_{ZZ}/2$ assumes centering the qubit frequency. This gives $\langle\phi^2\rangle = (\Omega_{ZZ}t_{\text{gate}})^2/4$, and since for RB, the error per gate is $E = \langle\phi^2\rangle/6$ [see Eq. (A3)], we arrive at Eq. (5) for the error per gate due to the Ω_{ZZ} interaction,

$$E = \frac{\pi^2}{6} \left(\frac{\Omega_{ZZ}}{2\pi} t_{\text{gate}} \right)^2. \quad (\text{G5})$$

TABLE III. Gate error fit parameters.

Gate	Linear term (10^{-6} error/ns)	Quadratic term (10^{-6} error/ns ²)
I	17	0.22
XX	20	...
Z	24	0.18
YX	22	...

APPENDIX H: FITS TO GATE ERRORS IN FIG. 4

For the data in the Fig. 4, the fits are made either to a simple linear model in the case of Markovian noise (the XX and YX cases) or to a quadratic and linear model in the case of non-Markovian noise (the I and Z cases). There is no offset in any fit. See Table III.

Note that the contribution from $T_1 = 26.7 \mu\text{s}$ to the linear portion of the error, given by Eq. (A4), is 9.3×10^{-6} error/ns or roughly half of the error measured. The remainder is equivalent to a white-noise dephasing with time constant $T_{\text{white}} \approx 30 \mu\text{s}$, according to Eqs. (A3) and (B3). The quadratic terms correspond with $T_{\phi_2} \approx 1 \mu\text{s}$.

APPENDIX I: TELEGRAPH NOISE MEASURED IN OTHER DEVICES

Telegraph noise is observed in many other devices. In Fig. 7, we present RB Ramsey measurements of three other devices that show telegraph noise, with the data from Fig. 2 reproduced for reference (a); one is another device on the

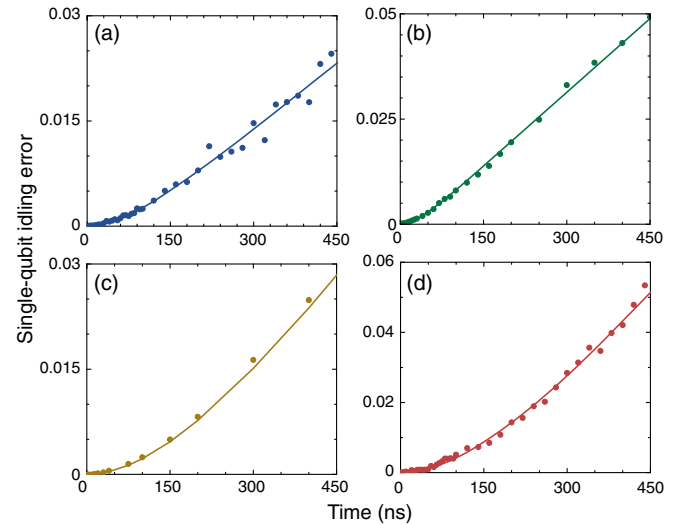


FIG. 7. Telegraph noise measured with the RB Ramsey experiment in other devices. All fits include T_1 and telegraph noise only [Eq. (4)]. (a) A reproduction of Fig. 2 data for reference. (b) Measurement of another Xmon on the same chip as the device. (c) Measurement of an Xmon qubit from another sample; see Ref. [23] for device details. (d) Measurement of a gmon qubit; see Ref. [47] for device details.

TABLE IV. Fits for telegraph noise measured in other devices (Fig. 7); see text and references for sample details.

Sample (see text)	f_{10} (GHz)	$df/d\Phi$ (GHz/ Φ_0)	T_1 (μ s)	T_{sw} (ns)	Δf_{10} (kHz)	Device Details
a	4.9	4.81	26.7	84	479	q2 of Ref. [24]
b	4.8	5.36	15.7	183	274	q0 of Ref. [24]
c	5.5	3.96	22.2	201	199	q2 of Ref. [23]
d	4.9	6.62	15.7	32	528	q1 of Ref. [47]

same chip (b), one another Xmon with different parameters [23] (c), and the last a gmon qubit [47] (d). All fits are to T_1 and telegraph noise only, Eq. (4), with fit parameters given in Table IV.

- [1] Frederick C. Wellstood, Cristian Urbina, and John Clarke, Low-frequency noise in dc superconducting quantum interference devices below 1 K, *Appl. Phys. Lett.* **50**, 772 (1987).
- [2] Crispin W. Gardiner and Peter Zoller, *Quantum Noise: A Handbook of Markovian and Non-Markovian Quantum Stochastic Methods with Applications to Quantum Optics*, 3rd ed. (Springer, New York, 2004).
- [3] E. Hahn, Spin echoes, *Phys. Rev.* **80**, 580 (1950).
- [4] Audrey Cottet, Ph.D. thesis, Université Paris VI, 2002.
- [5] Michael Biercuk, Hermann Uys, Aaron VanDevender, Nobuyasu Shiga, Wayne Itano, and John Bollinger, Experimental Uhrig dynamical decoupling using trapped ions, *Phys. Rev. A* **79**, 062324 (2009).
- [6] Jonas Bylander, Simon Gustavsson, Fei Yan, Fumiki Yoshihara, Khalil Harrabi, George Fitch, David G. Cory, Yasunobu Nakamura, Jaw-Shen Tsai, and William D. Oliver, Noise spectroscopy through dynamical decoupling with a superconducting flux qubit, *Nat. Phys.* **7**, 565 (2011).
- [7] E. Knill, D. Leibfried, R. Reichle, J. Britton, R. B. Blakestad, J. D. Jost, C. Langer, R. Ozeri, S. Seidelin, and D. J. Wineland, Randomized benchmarking of quantum gates, *Phys. Rev. A* **77**, 012307 (2008).
- [8] C. A. Ryan, M. Laforest, and R. Laflamme, Randomized benchmarking of single- and multi-qubit control in liquid-state NMR quantum information processing, *New J. Phys.* **11**, 013034 (2009).
- [9] Easwar Magesan, J. M. Gambetta, and Joseph Emerson, Scalable and Robust Randomized Benchmarking of Quantum Processes, *Phys. Rev. Lett.* **106**, 180504 (2011).
- [10] K. R. Brown, A. C. Wilson, Y. Colombe, C. Ospelkaus, A. M. Meier, E. Knill, D. Leibfried, and D. J. Wineland, Single-qubit-gate error below 10^{-4} in a trapped ion, *Phys. Rev. A* **84**, 030303 (2011).
- [11] Jay M. Gambetta, A. D. Córcoles, S. T. Merkel, B. R. Johnson, J. A. Smolin, Jerry M. Chow, C. A. Ryan, Chad Rigetti, S. Poletto, T. A. Ohki, Mark B. Ketchen, and M. Steffen, Characterization of Addressability by Simultaneous Randomized Benchmarking, *Phys. Rev. Lett.* **109**, 240504 (2012).
- [12] A. D. Córcoles, Jay M. Gambetta, Jerry M. Chow, John A. Smolin, Matthew Ware, Joel Strand, B. L. T. Plourde, and M. Steffen, Process verification of two-qubit quantum gates by randomized benchmarking, *Phys. Rev. A* **87**, 030301 (2013).
- [13] Fei Yan, Simon Gustavsson, Jonas Bylander, Xiaoyue Jin, Fumiki Yoshihara, David G. Cory, Yasunobu Nakamura, Terry P. Orlando, and William D. Oliver, Rotating-frame relaxation as a noise spectrum analyser of a superconducting qubit undergoing driven evolution, *Nat. Commun.* **4**, 2337 (2013).
- [14] Daniel Sank, R. Barends, Radoslaw C. Bialczak, Yu Chen, J. Kelly, M. Lenander, E. Lucero, Matteo Mariantoni, A. Megrant, M. Neeley, P. J. J. O'Malley, A. Vainsencher, H. Wang, J. Wenner, T. C. White, T. Yamamoto, Yi Yin, A. N. Cleland, and John M. Martinis, Flux Noise Probed with Real Time Qubit Tomography in a Josephson Phase Qubit, *Phys. Rev. Lett.* **109**, 067001 (2012).
- [15] Fei Yan, Jonas Bylander, Simon Gustavsson, Fumiki Yoshihara, Khalil Harrabi, David G. Cory, Terry P. Orlando, Yasunobu Nakamura, Jaw-Shen Tsai, and William D. Oliver, Spectroscopy of low-frequency noise and its temperature dependence in a superconducting qubit, *Phys. Rev. B* **85**, 174521 (2012).
- [16] T. P. Harty, D. T. C. Allcock, and C. J. Ballance, High-Fidelity Preparation, Gates, Memory and Readout of a Trapped-Ion Quantum Bit, *Phys. Rev. Lett.* **113**, 220501 (2014).
- [17] Hanhee Paik, D. I. Schuster, Lev S. Bishop, G. Kirchmair, G. Catelani, A. P. Sears, B. R. Johnson, M. J. Reagor, L. Frunzio, L. I. Glazman, S. M. Girvin, M. H. Devoret, and R. J. Schoelkopf, Observation of High Coherence in Josephson Junction Qubits Measured in a Three-Dimensional Circuit QED Architecture, *Phys. Rev. Lett.* **107**, 240501 (2011).
- [18] Chad Rigetti, Jay M. Gambetta, Stefano Poletto, B. L. T. Plourde, Jerry M. Chow, A. D. Córcoles, John A. Smolin, Seth T. Merkel, J. R. Rozen, George A. Keefe, Mary B. Rothwell, Mark B. Ketchen, and M. Steffen, Superconducting qubit in a waveguide cavity with a coherence time approaching 0.1 ms, *Phys. Rev. B* **86**, 100506 (2012).
- [19] T. Choi, S. Debnath, T. A. Manning, C. Figgatt, Z.-X. Gong, L.-M. Duan, and C. Monroe, Optimal Quantum Control of Multimode Couplings between Trapped Ion Qubits for Scalable Entanglement, *Phys. Rev. Lett.* **112**, 190502 (2014).
- [20] Philipp Schindler, Daniel Nigg, Thomas Monz, Julio T. Barreiro, Esteban Martinez, Shannon X. Wang, Stephan Quint, Matthias F. Brandl, Volckmar Nebendahl, Christian F. Roos, Michael Chwalla, Markus Hennrich, and Rainer Blatt, A quantum information processor with trapped ions, *New J. Phys.* **15**, 123012 (2013).
- [21] D. D. Awschalom, L. C. Bassett, and A. S. Dzurak, Quantum spintronics: Engineering and manipulating atom-like spins in semiconductors, *Science* **339**, 1174 (2013).

- [22] J. T. Muhonen *et al.*, Quantifying the quantum gate fidelity of single-atom spin qubits in silicon by randomized benchmarking, *J. Phys. Condens. Matter* **27**, 154205 (2015).
- [23] R. Barends *et al.*, Superconducting quantum circuits at the surface code threshold for fault tolerance, *Nature (London)* **508**, 500 (2014).
- [24] J. Kelly *et al.*, State preservation by repetitive error detection in a superconducting quantum circuit, *Nature (London)* **519**, 66 (2015).
- [25] John M. Martinis, S. Nam, J. Aumentado, K. M. Lang, and C. Urbina, Decoherence of a superconducting qubit due to bias noise, *Phys. Rev. B* **67**, 094510 (2003).
- [26] R. Barends, J. Kelly, A. Megrant, D. Sank, E. Jeffrey, Y. Chen, Y. Yin, B. Chiaro, J. Mutus, C. Neill, P. O'Malley, P. Roushan, J. Wenner, T. C. White, A. N. Cleland, and John M. Martinis, Coherent Josephson Qubit Suitable for Scalable Quantum Integrated Circuits, *Phys. Rev. Lett.* **111**, 080502 (2013).
- [27] In Refs. [23, 28], the convention was used where $g/2\pi$ is the swap rate. Here we use $2g/2\pi$ as the swap rate, in accordance with others in the field.
- [28] J. Kelly *et al.*, Optimal Quantum Control Using Randomized Benchmarking, *Phys. Rev. Lett.* **112**, 240504 (2014).
- [29] Evan Jeffrey, Daniel Sank, J. Y. Mutus, T. C. White, J. Kelly, R. Barends, Y. Chen, Z. Chen, B. Chiaro, A. Dunsworth, A. Megrant, P. J. J. O'Malley, C. Neill, P. Roushan, A. Vainsencher, J. Wenner, A. N. Cleland, and John M. Martinis, Fast Accurate State Measurement with Superconducting Qubits, *Phys. Rev. Lett.* **112**, 190504 (2014).
- [30] Easwar Magesan, Jay M. Gambetta, B. R. Johnson, Colm A. Ryan, Jerry M. Chow, Seth T. Merkel, M. P. da Silva, George A. Keefe, Mary B. Rothwell, Thomas A. Ohki, Mark B. Ketchen, and M. Steffen, Efficient Measurement of Quantum Gate Error by Interleaved Randomized Benchmarking, *Phys. Rev. Lett.* **109**, 080505 (2012).
- [31] E. Paladino, L. Faoro, G. Falci, and Rosario Fazio, Decoherence and $1/f$ Noise in Josephson Qubits, *Phys. Rev. Lett.* **88**, 228304 (2002).
- [32] Alexander Shnirman, Gerd Schön, Ivar Martin, and Yuri Makhlin, Low- and High-Frequency Noise from Coherent Two-Level Systems, *Phys. Rev. Lett.* **94**, 127002 (2005).
- [33] F. Yoshihara, K. Harrabi, A. O. Niskanen, Y. Nakamura, and J. S. Tsai, Decoherence of Flux Qubits due to $1/f$ Flux Noise, *Phys. Rev. Lett.* **97**, 167001 (2006).
- [34] Radoslaw C. Bialczak, R. McDermott, M. Ansmann, M. Hofheinz, N. Katz, Erik Lucero, Matthew Neeley, A. D. O'Connell, H. Wang, A. N. Cleland, and John M. Martinis, $1/f$ Flux Noise in Josephson Phase Qubits, *Phys. Rev. Lett.* **99**, 187006 (2007).
- [35] S. Sendelbach, D. Hover, A. Kittel, M. Mück, John M. Martinis, and R. McDermott, Magnetism in SQUIDs at Millikelvin Temperatures, *Phys. Rev. Lett.* **100**, 227006 (2008).
- [36] M. Bal, M. H. Ansari, J. L. Orgiazzi, R. M. Lutchyn, and A. Lupascu, Dynamics of parametric fluctuations induced by quasiparticle tunneling in superconducting flux qubits, arXiv:1406.7350.
- [37] D. Ristè, C. C. Bultink, M. J. Tiggelman, R. N. Schouten, K. W. Lehnert, and L. DiCarlo, Millisecond charge-parity fluctuations and induced decoherence in a superconducting transmon qubit, *Nat. Commun.* **4**, 1913 (2013).
- [38] A. P. Sears, A. Petrenko, G. Catelani, L. Sun, Hanhee Paik, G. Kirchmair, L. Frunzio, L. I. Glazman, S. M. Girvin, and R. J. Schoelkopf, Photon shot noise dephasing in the strong-dispersive limit of circuit QED, *Phys. Rev. B* **86**, 180504 (2012).
- [39] M. Stern, G. Catelani, Y. Kubo, C. Grezes, A. Bienfait, D. Vion, D. Esteve, and P. Bertet, Flux Qubits with Long Coherence Times for Hybrid Quantum Circuits, *Phys. Rev. Lett.* **113**, 123601 (2014).
- [40] Y. M. Galperin, B. L. Altshuler, J. Bergli, and D. V. Shantsev, Non-Gaussian Low-Frequency Noise as a Source of Qubit Decoherence, *Phys. Rev. Lett.* **96**, 097009 (2006).
- [41] G. Ithier, E. Collin, P. Joyez, P. J. Meeson, D. Vion, D. Esteve, F. Chiarello, A. Shnirman, Y. Makhlin, J. Schrieffer, and G. Schön, Decoherence in a superconducting quantum bit circuit, *Phys. Rev. B* **72**, 134519 (2005).
- [42] L. DiCarlo, J. M. Chow, J. M. Gambetta, Lev S. Bishop, B. R. Johnson, D. I. Schuster, J. Majer, a. Blais, L. Frunzio, S. M. Girvin, and R. J. Schoelkopf, Demonstration of two-qubit algorithms with a superconducting quantum processor, *Nature (London)* **460**, 240 (2009).
- [43] Andrei Galiatdinov, Alexander N. Korotkov, and John M. Martinis, Resonator-zero-qubit architecture for superconducting qubits, *Phys. Rev. A* **85**, 042321 (2012).
- [44] Alexandre Blais, Ren-Shou Huang, Andreas Wallraff, S. M. Girvin, and R. J. Schoelkopf, Cavity quantum electrodynamics for superconducting electrical circuits: An architecture for quantum computation, *Phys. Rev. A* **69**, 062320 (2004).
- [45] Jens Koch, Terri M. Yu, Jay Gambetta, A. A. Houck, D. I. Schuster, J. Majer, Alexandre Blais, M. H. Devoret, S. M. Girvin, and R. J. Schoelkopf, Charge-insensitive qubit design derived from the Cooper pair box, *Phys. Rev. A* **76**, 042319 (2007).
- [46] Erik Lucero, Julian Kelly, Radoslaw C. Bialczak, Mike Lenander, Matteo Mariantoni, Matthew Neeley, A. D. O'Connell, Daniel Sank, H. Wang, Martin Weides, James Wenner, Tsuyoshi Yamamoto, A. N. Cleland, and John M. Martinis, Reduced phase error through optimized control of a superconducting qubit, *Phys. Rev. A* **82**, 042339 (2010).
- [47] C. Neill (to be published).